

Various effects of magnetite on international simple glass (ISG) dissolution: implications for the long-term durability of nuclear glasses

Lindsey Neill, S. Gin, Thomas Ducasse, Trilce de Echave, Maxime Fournier, Patrick Jollivet, Alkiviadis Gourgiotis, Nathalie Wall

▶ **To cite this version:**

Lindsey Neill, S. Gin, Thomas Ducasse, Trilce de Echave, Maxime Fournier, et al.. Various effects of magnetite on international simple glass (ISG) dissolution: implications for the long-term durability of nuclear glasses. npj Materials Degradation, 2017, 1, pp.1. 10.1038/s41529-017-0001-6 . cea-02380473

HAL Id: cea-02380473

https://cea.hal.science/cea-02380473

Submitted on 26 Nov 2019

HAL is a multi-disciplinary open access archive for the deposit and dissemination of scientific research documents, whether they are published or not. The documents may come from teaching and research institutions in France or abroad, or from public or private research centers.

L'archive ouverte pluridisciplinaire **HAL**, est destinée au dépôt et à la diffusion de documents scientifiques de niveau recherche, publiés ou non, émanant des établissements d'enseignement et de recherche français ou étrangers, des laboratoires publics ou privés.



Distributed under a Creative Commons Attribution 4.0 International License

Various effects of magnetite on ISG glass dissolution: implication for the long-term durability of nuclear glasses

Lindsey Neill[a], Stéphane Gin[b], Thomas Ducasse[b], Trilce De Echave[b], Patrick Jollivet[b], Nathalie A. Wall[a]

[a]Chemistry Department, Washington State University, Pullman, WA 99163, USA

[b]CEA Marcoule, DTCD SECM, F-30207 Bagnols-sur-Cèze, France

Corresponding Authors: S. Gin: stephane.gin@cea.fr; N.A. Wall: nawall@wsu.edu

Abstract

Understanding the effect of near-field materials such as iron corrosion products on the alteration of vitreous nuclear waste is essential for modeling long-term stability of these waste forms in a geological repository. Monoliths with polished and as cut sides of International Simple Glass (ISG) – a six oxide borosilicate glass – were altered for 70 days in oxic conditions at 90 °C in a solution initially saturated in $^{29}SiO_2$ at pH 7; magnetite was then added to the leaching environment. Solution and solid analysis were performed to correlate the changes in the surface features and dissolution kinetics. It was found for the first time that magnetite primarily influences the mechanically constrained surface of the non-polished sides of the monoliths with little to no effect on the polished surfaces. This highlights the importance of the unique chemistry within cracks that invokes a drastic change in alteration from glass altered in environments containing iron corrosion products.

Keywords

Glass alteration; corrosion products; alteration layer; iron; magnetite; surface cracks

Introduction

Confinement within a borosilicate glass matrix is the currently proposed method of disposal of radionuclides remaining from used nuclear fuel from power reactors [1]. In France, the glass with about 18 wt% of waste is poured in a stainless steel canister. Before being disposed in a deep geological formation, the canister will be placed into a carbon steel over pack of a few cm thick [2]. A better understanding the interactions between glass and iron and iron corrosion products, is necessary to assess the performance of these waste forms and model the source term [3].

Over the last several decades, work has been performed to understand the fundamental mechanisms that control the glass dissolution process under a variety of conditions, and to link these mechanisms to the global kinetics [4]. The processes that control glass dissolution in a geological repository involve a complex set of reactions whose importance tremendously depends on the nature of the host rock, the near field materials [5,6], the temperature and the ground water composition and renewal rate, along with the glass composition [7–13] . The ultimate goal to parametric studies of glass alteration under a variety of conditions is build a predictive model that can account for the kinetics of long-term alteration [14–16]. Since experimental validation of the predictive models under accelerated conditions is not possible as glass dissolution is controlled by coupled non linear processes (Poinssot and Gin JNM), ,validation relies on the study of archeological and basaltic glasses [17–19]. A thorough understanding of all mechanisms and kinetics must be achieved to build a robust model.

Literature pertaining to borosilicate glass dissolution demonstrates that silica species play a large role in the mechanisms and associated kinetics. In diluted conditions water begins to diffuse into the glass matrix (hydration) [20] and alkali ions begin to exchange with the positively charged hydrogen species (interdiffusion) [21–23] (equation 1). Hydrolysis of the silicon network

also begins with silica being released into solution [24,25] (equation 2 and 3). The corresponding kinetic regime is designated as the *initial* or *forward rate* and is denoted by r_0.

$$\text{-Si-O-M}^+ + \text{H}^+ \rightarrow \text{Si-O}^- + \text{M}^+ + \text{OH}^- \quad \text{Equation 1}$$

$$\text{-Si-O}^- + \text{H}_2\text{O} \rightarrow \text{Si-OH} + \text{OH}^- \quad \text{Equation 2}$$

$$\text{Si-O-S(OH)}_3 + \text{OH}^- \rightarrow \text{H}_4\text{SiO}_4 + \text{Si-O}^- \quad \text{Equation 3}$$

As the silica concentration in solution increases, the rate slows into a *residual rate* denoted by r_r. The decrease in rate is attributed both to the decrease of the affinity of the reaction of hydrolysis of the silicate network and to the formation of a gel layer that becomes transport limiting [26]. Two different mechanisms are proposed for the formation of this gel layer. One is based on the precipitation of a silica rich layer on the glass surface. The second is due to in-situ recondensation of the silicon oxygen bonds which forms a porous gel layer on the glass surface. Previous studies have used isotopic tracers to differentiate between these mechanisms, allowing a greater understanding of the exchange of silicon between the bulk solution and glass surface [27–30]. These studies showed that only one single mechanism may not be responsible for the residual rate but a combination of these mechanisms that are heavily dependent on the solution pH.

There is also a possibility of an alteration resumption, commonly attributed to the rapid precipitation of secondary phases [31]. In this regime, zeolithes and calcium silicate hydrates form at the expense of the passivating film. Additionally, environmental complexants, such as organic molecules or iron corrosion products, can have detrimental effects on the passivating layer [32,33]. Glass compositions, such as those high in aluminum, and solution pH are two key factors controlling this regime [34].

Some of the above listed mechanisms are still under investigation, especially at small scale following the aim to link the basic mechanisms to the three main kinetic regimes (initial rate, residual rate, resumption of alterarion) [4]. As said above, many factors can influence the kinetics such as pH, temperature, solution conditions, and environmental factors (i.e. near-field materials [35]).

Iron and the associated corrosion products (mainly siderite and magnetite [36] have been seen to enhance glass alteration both by the sorption of silica onto the surface of the iron-rich phases and by the precipitation of iron silicate [37–42]. Each of these different processes disturbs the equilibrium established between the glass surface layers and surrounding solution; these processes contribute to higher alteration rates for times depending on the amount and availability of iron in vicinity of the glass.

In addition to the processes listed above (sorption of silica on iron corrosion products and precipitation of iron silicates),[33] studied the effects of magnetite on SON68 glass – the French high level waste reference glass – and suggested that two other processes might take place: 1) precipitation of SiO_2 on the magnetite surface and 2) iron incorporation into the glass alteration layers with potential modifications of their transport properties. The present study gave evidence to each processes listed above except iron incorporation into the alteration layer which would be highly dependent on the iron available in solution due to dissolution of the magnetite. This demonstrates that the iron – glass relationship is complex and that much more information to understand these effects both on mechanisms and kinetics are needed.

Another factor that contributes to the durability of the glass is the formation of cracks on the glass surface, primarily because cracks increase the reactive surface area compare to a flat surface. The molten glass is poured into a stainless steel canister after the vitrification process. As the glass cools, cracks appear because of thermic shock due to a temperature gradient between the perimeter and core of the glass. At small scale, these cracks or defaults provide

preferential sites for alteration such as diffusion of alkali ions into the surrounding environment [43]

At laboratory scale, defaults within the glass matrix are also observed during cooling and sample preparation (e.g. cutting) [44,45]. These processes can be considered mechanically violent and generates a high number of micro cracks, or Griffith cracks [46] due to the metastable nature of the glass structure. Griffith summarized that the strength of the material was dependent on defects such as these surface cracks. These Griffith cracks can spontaneously propagate in time due to mechanical stress, chemical gradients, etc. The evolution of these micro cracks into larger cracks can be compared to dislocations in crystals due to grain boundaries. One method to remove these sample preparation artifacts is to use soft abrasion in the form of chemically polishing the glass surface. Though the types of defaults or surface cracks are caused by different methods, formation vs. processing, looking at alteration of non-polished glass surfaces can give insight into the alteration of the cracks seen in large-scale waste materials.

The goal of this study is to further understand the alteration of the glass waste form in the presence of iron corrosion products, specifically magnetite (Fe(II,III)Oxide). This study is an extension of a similar experiment performed. Experimental conditions of both works are similar, but the present work includes the addition of an iron source [28]. Comparison of results of this work with a reference experiment without an iron source, allows for a better understanding of the alteration layer properties. The experiment was carried out in condition initially saturated in ^{29}Si to follow the isotopic exchange of Si between the solution and glass to monitor changes of the alteration layer. Additionally, five of the six sides of the glass monoliths were left unpolished which gave insight into the effect of surface cracks on the alteration progress of the glass.

Results

Solution Analysis

Results from ICP-OES for individual glass constitutes and MC-ICP-MS for silicon isotopes are shown in Table 1.

Time	**$pH_{90°C}$**	**AGF**	**ICP-OES**						**MC-ICP-MS**			
Days		%	Si	B	Ca	Na	Fe	K	^{28}Si	^{29}Si	^{30}Si	^{TOT}Si
			$mg.L^{-1}$	$mg.L^{-1}$	$mg.L^{-1}$	$mg.L^{-1}$	$mg.L^{-1}$	$g.L^{-1}$	$mg.L^{-1}$	$mg.L^{-1}$	$mg.L^{-1}$	$mg.L^{-1}$
0.4	7.2	0	140.0	<0.1	0.9	6.3	BD	3.5	2.1	135.4	2.4	140.0
9	7.0	0.18	133.8	6.7	5.7	16.7	BD	3.7	-	-	-	-
14	7.2	0.21	139.7	8.1	7.3	20.2	BD	3.8	15.4	122.8	1.5	139.7
30	7.1	0.25	144.9	9.5	6.8	20.8	BD	3.7	16.7	126.7	1.6	144.9
62	7.1	0.29	149.2	10.9	9.2	23.5	BD	3.8	18.0	129.5	1.7	149.2
70	6.6	0.30	142.5	11.6	8.4	25.0	BD	3.0	8.0	133.3	1.3	142.6
71	7.0	0.30	81.2	11.8	12.9	29.7	BD	3.0	7.9	73.1	0.9	81.3
77	6.5	0.32	59.4	12.6	14.7	32.4	BD	2.9	6.7	51.6	0.8	59.1
84	6.7	0.32	48.1	12.6	11.9	32.8	BD	3.0	9.5	37.7	0.8	48.1
100	6.6	0.32	28.7	12.9	10.6	33.8	BD	3.1	7.7	20.4	0.6	28.7
126	6.9	0.37	22.6	15.2	9.8	37.6	BD	3.5	2.3	18.4	0.2	21.0
246	8.2	1.61	50.7	65.3	13.7	121.9	0.06	4.2	27.3	11.8	1.84	40.9
342	8.3	3.37	73.6	126.2	28.2	227.4	BD	3.7	-	-	-	-
395	8.5	4.68	81.3	149.6	29.0	278.8	BD	3.6	-	-	-	-

Table 1: ICP-OES and MC-ICP-MS analysis of solution sampled at various time points. BD indicates that the value for that element was below the 0.1 $mg.L^{-1}$ detection limit. Dotted line represents the addition of magnetite 'AGF' stands for Altered Glass Fraction and '-' within the MC-ICP-MS data denotes that the sample was not analyzed at that time point. There is a 10% uncertainty on each element measured by ICP-OES except Na which has a 50% error due to contamination within the K salts used to synthesize the potassium silicates during alkaline fusion. These potassium silicates were used to prepare the initial solution of 150 ppm Si. Elements measured by MC-ICP-MS have a 5% error due to matrix effects. The dotted horizontal line represents the addition of magnetite

Figure 1 shows the evolution of the silicon concentration along with the normalized loss based on boron solution conditions and pH throughout the experiment. The pH remained constant during the 150 first days by monitoring the solution and correcting to pH 7 by 0.5 M HNO_3 or 0.5

M KOH. At the last three time points, the pH slowly increased to approximately 8. Because this drift let the pH below orthosilicic acid starts dissociating into anions ($H_3SiO_4^-$, $H_2SiO_4^{2-}$…), this seems to have an insignificant effect on the studied system. Indeed, the glass dissolution rate, as shown in figure 2, remains essentially constant between day 126 and day 395.

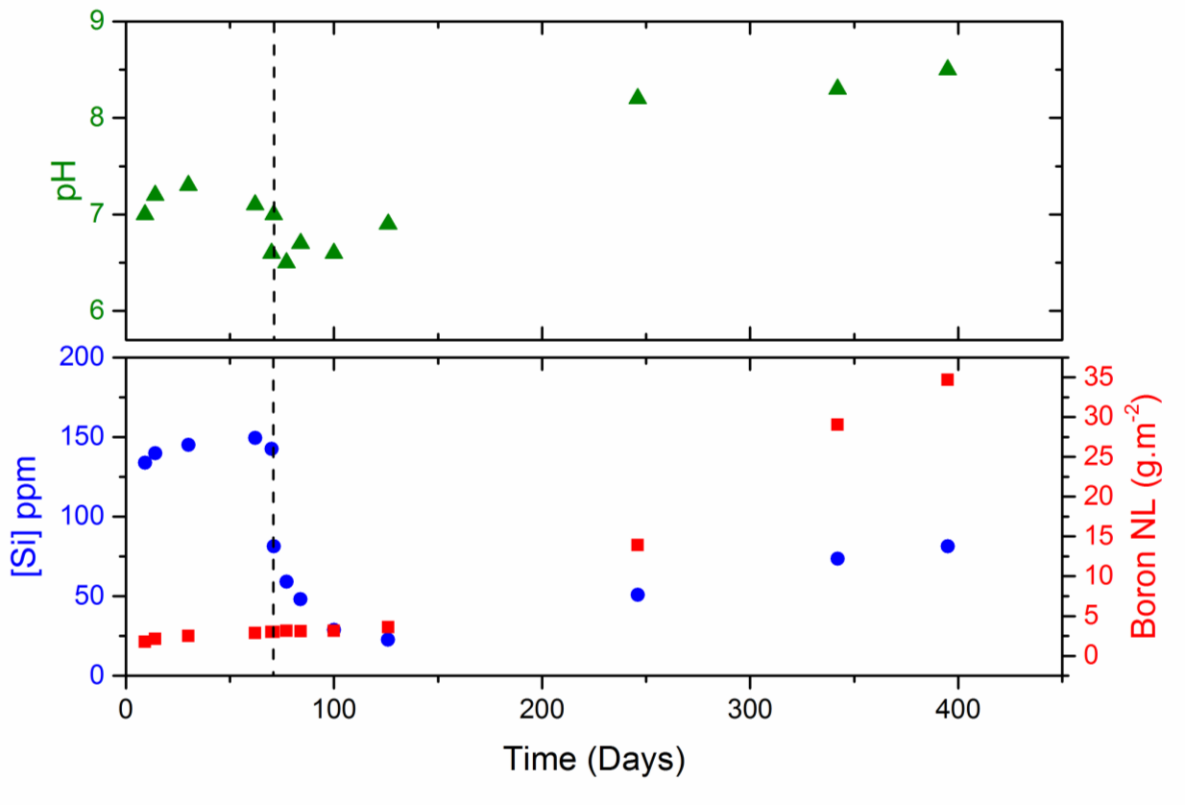


Figure 1: Upper graph shows the evolution of the pH (green triangles) during the experiment. At each time point the pH was corrected back to 7 after the initial measurement shown in the graph except for the last three time points. Lower graph shows the change in Si concentration (blue circles) and the normalized loss (red squares) calculated by boron concentration in solution. Resumption of alteration is seen at day 246 based on the increased concentration of boron and silicon in solution.

Over approximately the first two months, the glass was allowed to react in a solution saturated with amorphous silica under the same experimental conditions as seen in Gin et al 2015. This allowed for comparison to a long term study to determine the deviations in behavior after magnetite is added to the system. Magnetite was added 70 days after the experiment was initiated and a significant decrease in the concentration of silicon was observed almost

immediately with a decrease of approximately 60 ppm of silicon within the first day after magnetite addition. This decrease extends for two months after the addition of magnetite, at which point the solution only contains 22 ppm of silicon. The later time points extending to nine months after the addition of magnetite shows the resumption of alteration. Figure 2 presents the rate changes over the duration of the experiment based on the boron concentrations in solution.

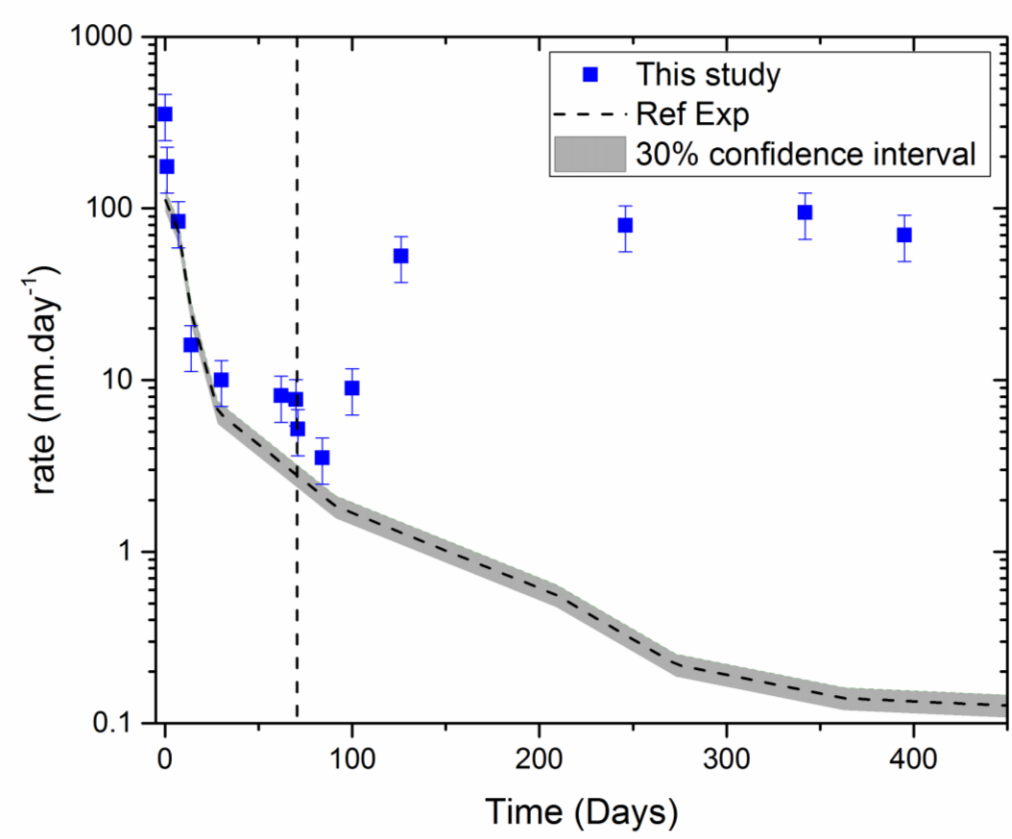


Figure 2: Rates of alteration calculated based on a linear regression of the equivalent thickness determined at each time point. The grey dotted line represents the rates seen within the reference experiment with a 30% confidence interval (gray shading). The black dotted line represents the addition of magnetite at day 70.

The rate continues to decrease after the addition of magnetite at day 70, although the rate never reaches the long term rates seen in Gin et al 2015 of 0.1 $nm.day^{-1}$. After ca. 100 days, the rate then increases. The rate then stays to a maximum of around 100 $nm.day^{-1}$ for the duration of the experiment. While this is a large increase, rates near the value calculated at day

one of this experiment (500 nm.day^{1}) were not seen even with silicon concentrations under the saturation value. Silicon isotopic concentrations were also monitored by MC-ICP-MS as shown in Figure 3.

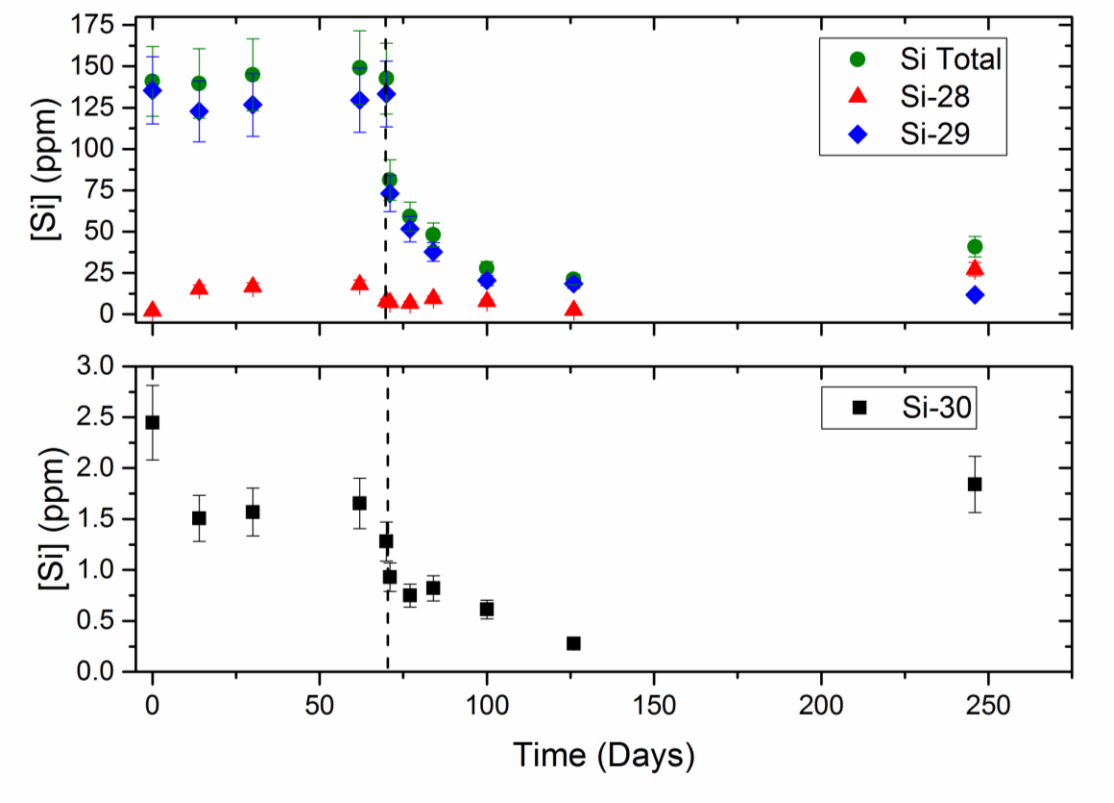


Figure 3: Evolution of Si concentration by isotope determined by analysis of the solution by MC-ICP-MS. The lower graph shows only Si-30 as it makes up less than 1% of the total Si concentration. The dotted black line represents the addition of magnetite at day 70.

Figure 3 demonstrates three different regimes. First, the system is in equilibrium, before the addition of magnetite, where surface layers form with no or little exchange with Si species present in the solution, as previously demonstrated [28]. The second regime lasts between days 70 – 126, during which the available Si in solution is consumed, either by sorption or precipitation on the magnetite surface or iron silicate precipitation. The third regime expands beyond 126 days. Si concentration increases though only ^{28}Si and ^{30}Si increase with ^{29}Si continues to decrease. This demonstrates that later time points are a resumption of alteration of

the glass itself. If the increased concentrations of Si were due to dissolution of the silicon early fixed onon the magnetite surface, ^{29}Si concentrations would have risen as well.

3.1 TOF-SIMS analysis of the glass monoliths

In addition to monitoring changes by solution analysis TOF-SIMS was used to qualitatively evaluate the changes of mobile elements within the alteration layer at four times throughout the experiment. Monoliths were withdrawn from the solution at day 70 (immediately before the addition of magnetite), day 84 (two weeks after addition), day 126 (two months after addition) and day 246 (almost six months after addition). Figure 4 shows the analysis of the polished face of the day 70 monolith with the three mobile species (B, Na, and Ca) showing anti-correlation behavior of the hydrous species represented by H. Sodium and calcium are known to exhibit this sigmoidal profile due to preferential dissolution of these elements, with similar behavior by boron [28]. While boron may not release by the same mechanisms as the alkali species, the low activation energy needed to break the B-O bonds (Zapol et al 2013) allows for the same profile to be seen.

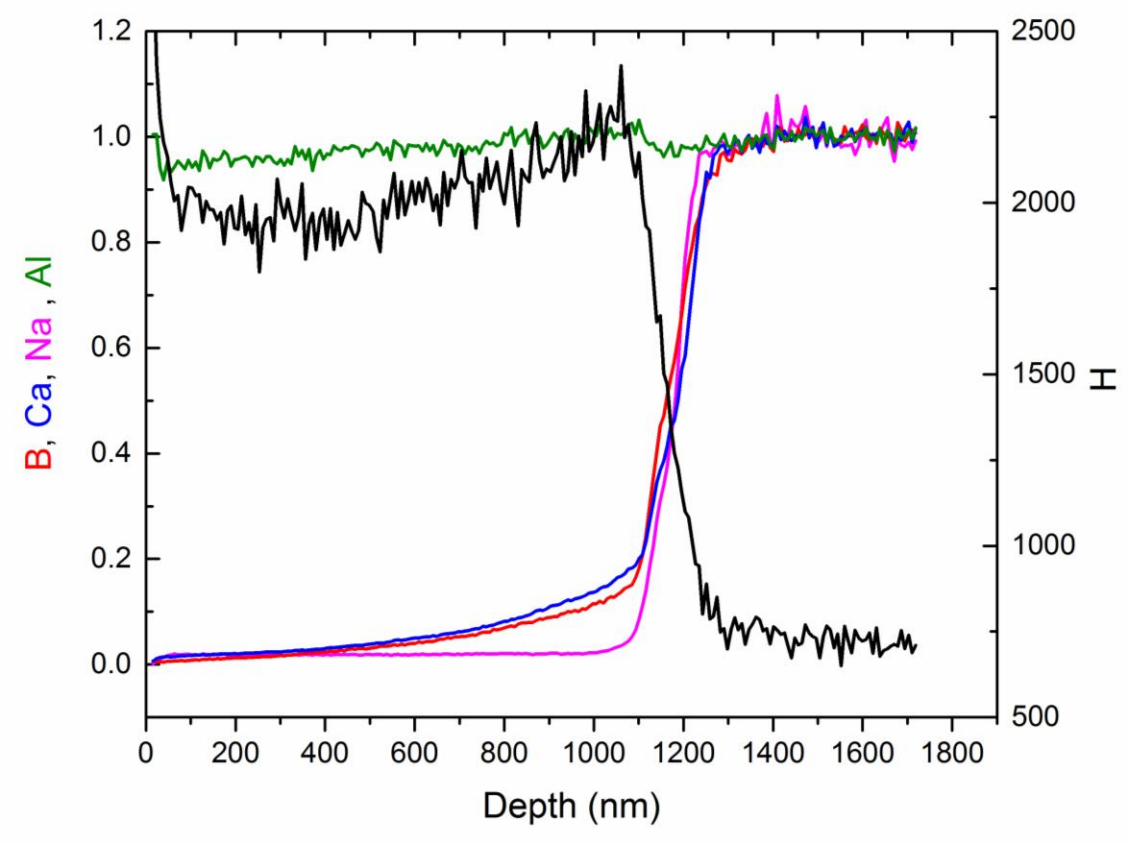


Figure 4: TOF-SIMS derived elemental profiles of the major glass constitutes of a monolith withdrawn at day 70, right before the addition of magnetite. This allows for a direct comparison of the monoliths with the reference experiment before the system was disturbed. All elements, except H, are normalized to Zr as this element is immobile during alteration and to their concentration in the pristine glass, with allows for a qualitative comparison between the elements.

The potential inclusion of iron into the alteration layers formed on the polished face of the monoliths were also studied by TOF-SIMS in Figure 5. Significant iron incorporation into the alteration layer is not seen until day 246. Monoliths from day 83 and 126 do show an increase of iron within the first couple nanometers of the sample but this could be contributed to magnetite grains adhering to the surface instead of being incorporated into the alteration layer. While iron containing secondary phases are commonly observed in previous studies, these results suggest that iron incorporation happens secondarily to the reactions that occur at the magnetite surface. This could also be due to the time it takes for the dissolution of magnetite to introduce iron into

the solution since the magnetite and glass surfaces were not in contact. Importantly, these profiles also show that there is not a significant increase in alteration layer thickness, based on the boron profile, even after the addition of magnetite and calculated resumption of alteration. Since only the polished side of the monolith was analyzed by TOF-SIMS, this suggests that the behavior of the polished and unpolished sides strongly differ to account for this observation. This will be discussed further later in this paper.

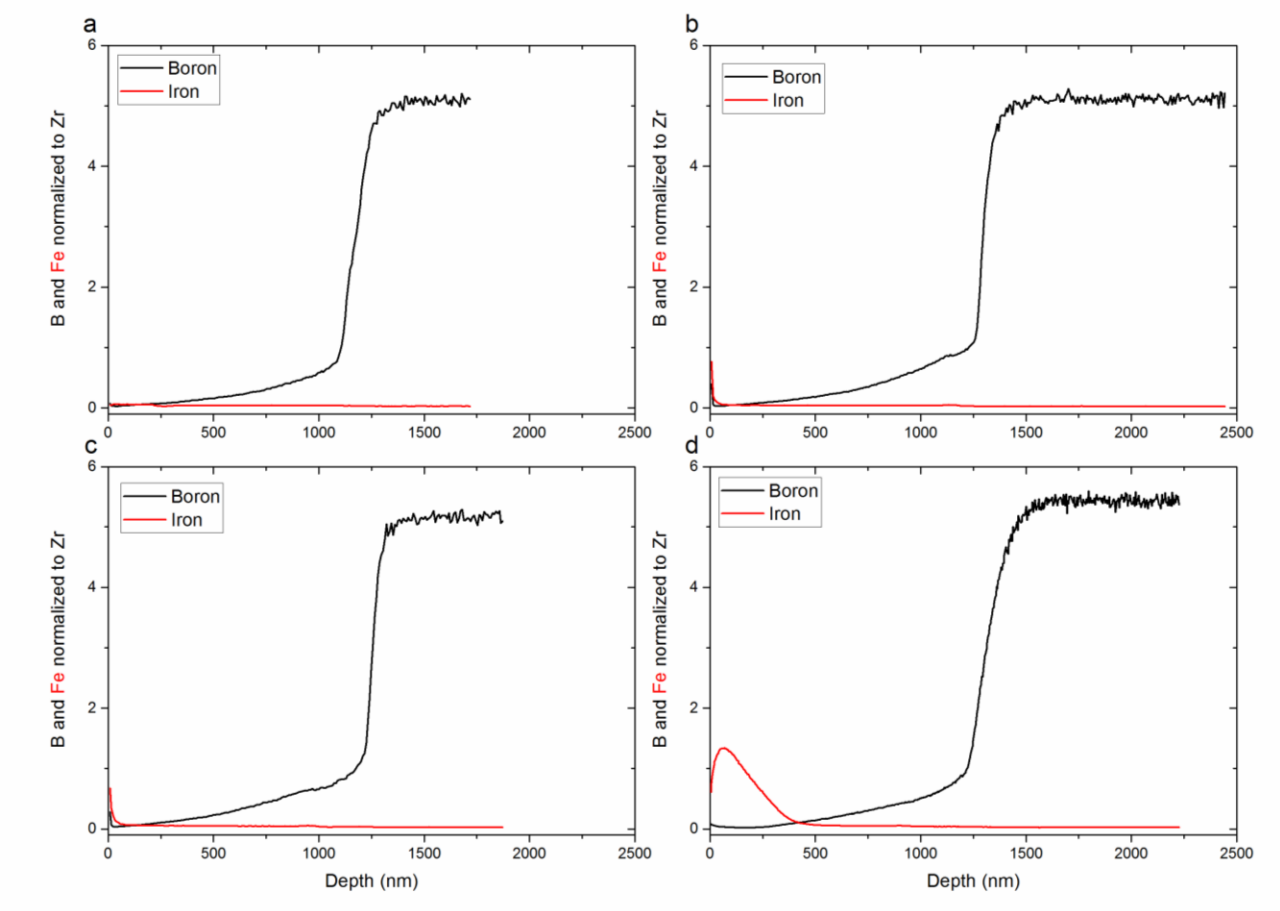


Figure 5: TOF-SIMS elements profiles for iron (red) and boron (black) of the polished surface of each monolith. The boron profile is shown as a measurement of the alteration layer thickness at each time point. a) day 70: before addition of magnetite E_{th} = 1.17 µm b) day 83: two weeks after addition E_{th} = 1.29 µm c) day 126: two months after addition E_{th} = 1.25 µm d) day 246: 6 months after addition E_{th} = 1.26 µm. Depths were measured by profilometry during TOF-SIMS analysis.

TEM/SEM of glass and magnetite surfaces

Polished faces of the monoliths withdrawn at day 70, 84, and 126 were analyzed by SEM to monitor the growth of secondary phases and any surface features. The monolith withdrawn at day 246 was analyzed by TEM. Figure 6 shows images from the day 126 sample of tilted samples It was not seen secondary phases on the surface of a monolith until day 126 that EDS and XRD analysis show the secondary phases observed on the 126 day sample are amorphous and contain elements common to the glass composition. No iron containing secondary phases were seen at these points in time. In addition to the images displayed in Figure 7, a cross section of the same monolith was analyzed by SEM to calculate the alteration layer thickness at this time point (1.26 µm).

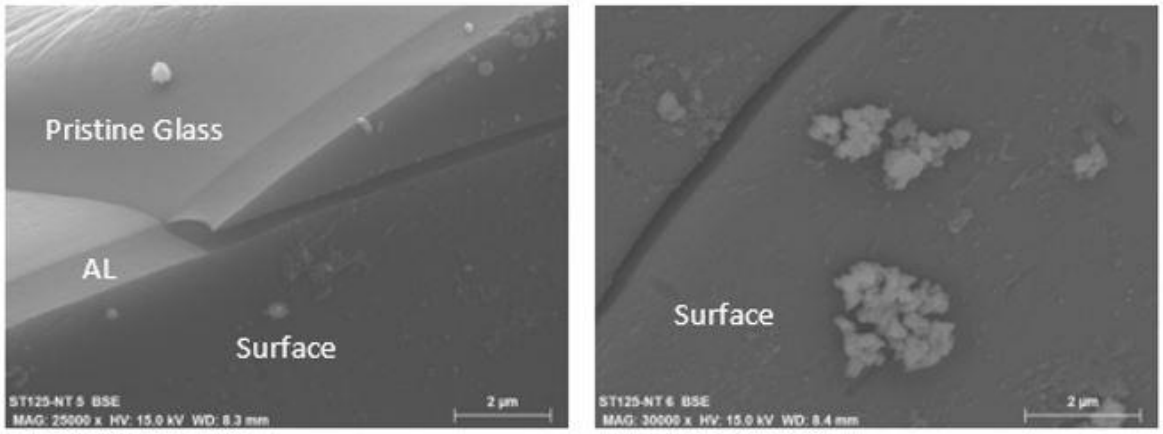


Figure 6: SEM image of polished surface of day 126 monolith. Secondary phases not seen on previous samples have begun to form. Left image shows all three portions of the glass (pristine, alteration layer, and surface). The image on the right shows a close up of the secondary phases seen on the surface.

Figure 7 shows the TEM image of a monolith withdrawn at day 246. This shows an alteration layer thickness of 1 µm with an additional 300 nm of secondary phases. Electron diffraction analysis showed that no crystalline phases were present in the alteration layer of the day 246 monolith. EDS analysis could not identify the secondary phases due to the presence of large quantities of the deposited metals such as gold and platinum.

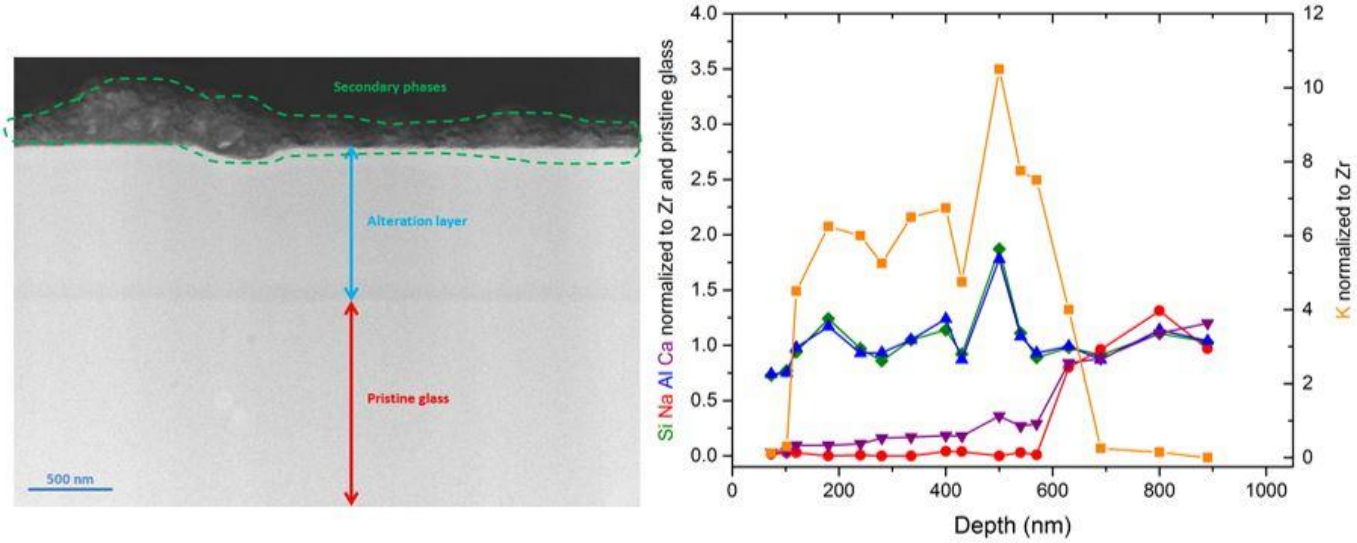


Figure 7: TEM image on the left of polished side of day 246 monolith. Alteration layer of approximately 1 µm is seen with an additional 300 nm of secondary phases on the surface. The absence of contrast inside the alteration layer shows that there is no porosity yet formed within the alteration layer or that the pore size is inferior to 5 – 10 nm. The right figure shows the EDS profile of this alteration region.

SEM analysis of a monolith withdrawn from the experiment at day 358 showed that significant changes at the glass surface happened at the final time point of the experiment. Figure 8 shows the alteration layers on the non-polished surfaces of the monolith that now contain sections of large amounts of alteration associated with cracks in the glass surface. These cracks prove to be a critical feature in the alteration of the glass surface. The majority of the alteration takes place primarily at these points instead of a uniform alteration across all surfaces as there does not seem to be a change in alteration thickness on the polished surface. EDS mapping shows an additional layer containing iron on the glass surface.

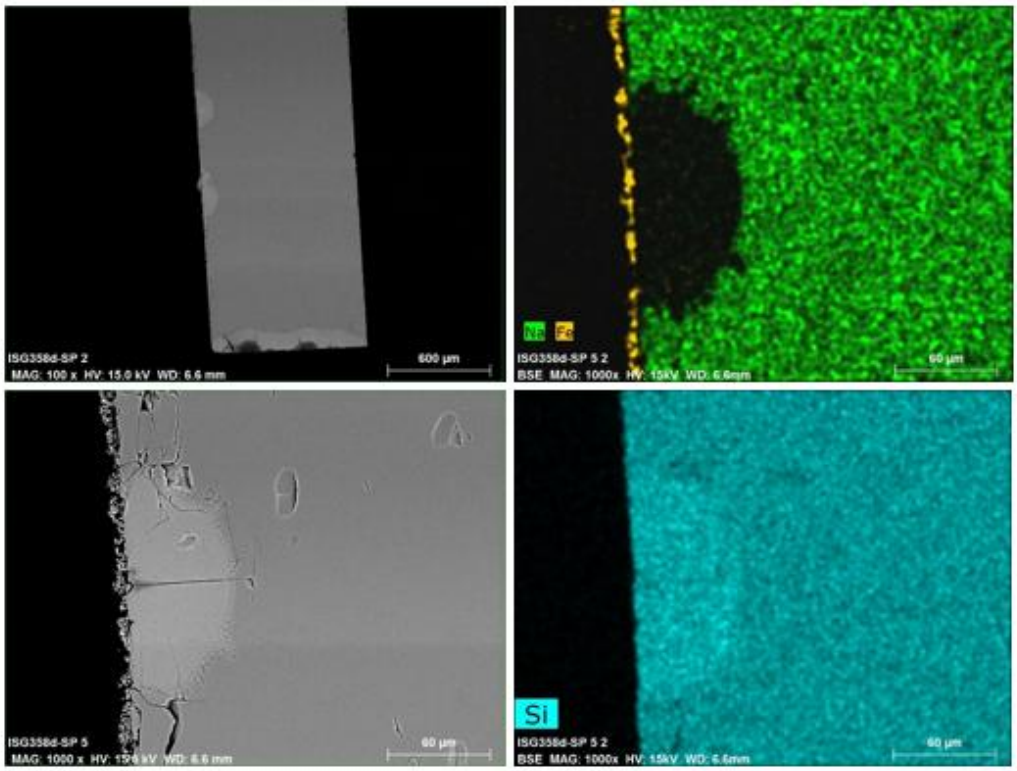


Figure 8: SEM images of day 358 monolith. In the upper left, the total monolith is shown with the polished side on the right. Areas of enhanced alteration are seen on all unpolished surfaces. Bottom left shows a close up of one of these areas of alteration that surrounds a crack in the surface. The images on the right show EDS mapping of significant ions denoting the alteration area and an iron rich area on the surface that is silicon poor.

TEM and SEM observations were also performed on a sample of magnetite withdrawn at day 246; results are presented with Figure 9.

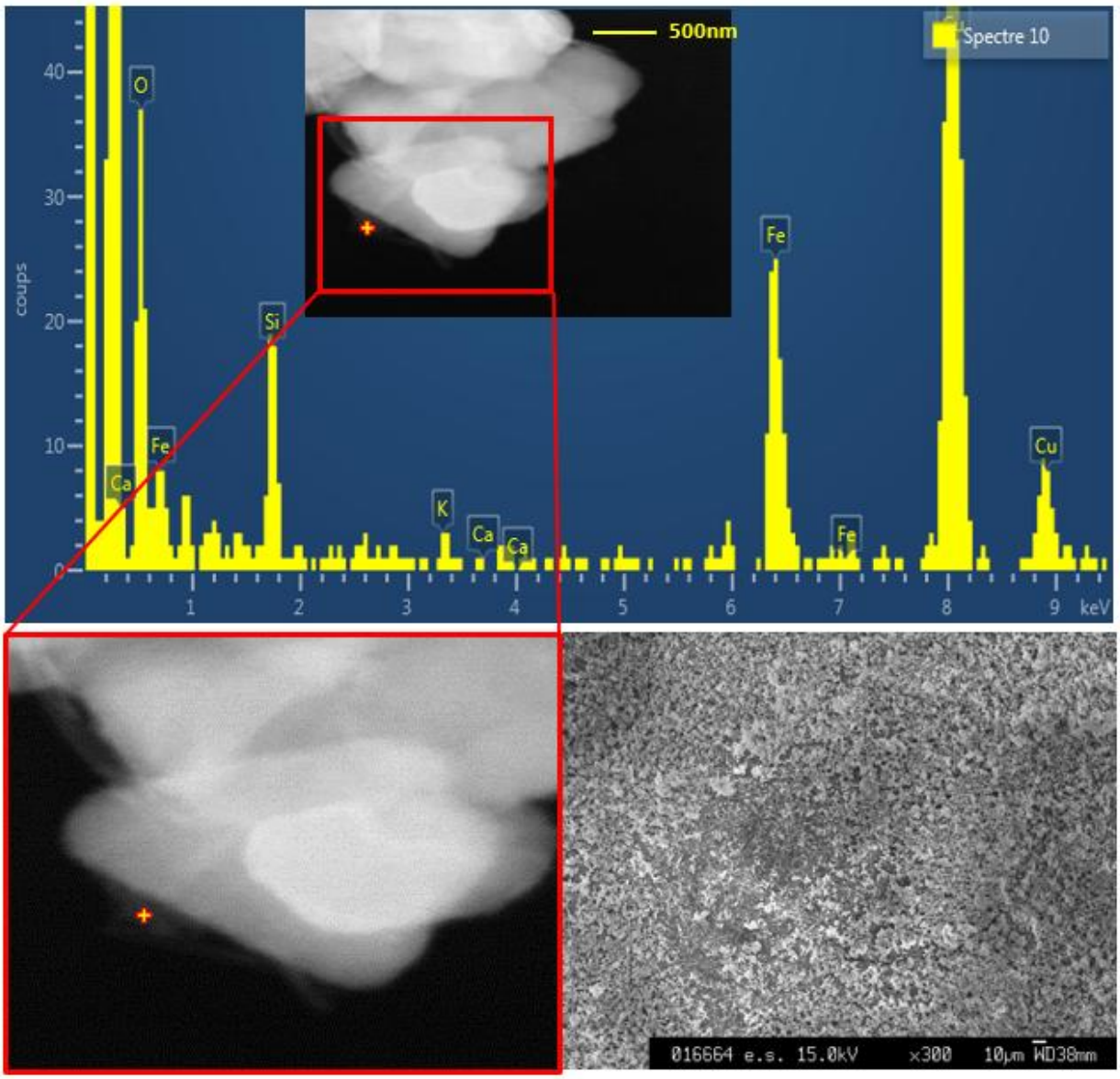


Figure 9: TEM image and EDS analysis of one magnetite grain is shown at the top with a zoom of the edge of the magnetite grain at the bottom left. High concentrations of Cu are seen due to metallic coating during sample preparation. Silicon peaks are seen along with potassium and calcium which indicate that silicates are precipitating on the surface of the magnetite in addition to silicon sorption. Bottom right figure shows an SEM image of these silicates covering the surface of the magnetite grain.

TEM EDS analysis shows clusters with increased concentrations of silicon outside the grain boundary confirming the precipitation of silica or iron silicate on the surface of the magnetite.

SEM images show the entire surface of the magnetite grains is covered with a Si-rich secondary phase.

Behavior of diffusive species

In an attempt to further understand the diffusivity changes within the alteration layer formed on the polished face of monoliths withdrawn at days 70, 84, 126, and 246 were subjected to a post-tracing experiment as outlined in methods. The behavior of iron into the surface as well as methylene blue, a molecule of approximately 1 nm in diameter, and Li, which has been shown to diffuse into the pristine glass at a rate higher than other hydrous species (Neeway et al 2014), were monitored. Figure 10 shows a comparison of a monolith before the addition of magnetite and six months after magnetite addition (at which time iron was seen incorporated into the alteration layer). Since these components are not within the glass composition they cannot be normalized and thus only give a qualitative view of diffusion into the alteration layers. At day 70, just before the addition of magnetite, only lithium diffusion is seen suggesting the pores diameters are too small to allow ingress of large molecules. Methylene blue is seen only within the first few nm, implying that only molecules of the dye are adhering the outside of the monolith instead of diffusing into the alteration layers. These results are consistent with those published in the literature [28,29]. They confirm that a dense layer made of subnanoporous amorphous silica acts as a molecular sieve for aqueous species. At day 246, two distinct layers are seen; one with increased iron concentrations and the common alteration layer seen at all time points. Lithium is seen to partition between these two layers with a decrease at the alteration layer pristine glass interface while still incorporating into the gel layer and into the pristine glass. Methylene blue is also present in the secondary iron layer up to the interface of these two alteration layers. In the reference experiment, methylene blue was also seen to diffuse up to 250 nm of a monolith sampled at day 209. Since this 250 nm cutoff was seen in both the

reference experiment and currently with iron introduction, it suggests that iron is not responsible for this secondary layer but only this outer 250 nm contain pores with diameters large enough to incorporate larger ions. Although there is this significant interface between an iron rich layer and the common alteration layer, this is most likely due to the nature of the alteration layer and pore diameters of this region instead of an iron affecting the properties or porosity of the alteration layer itself.

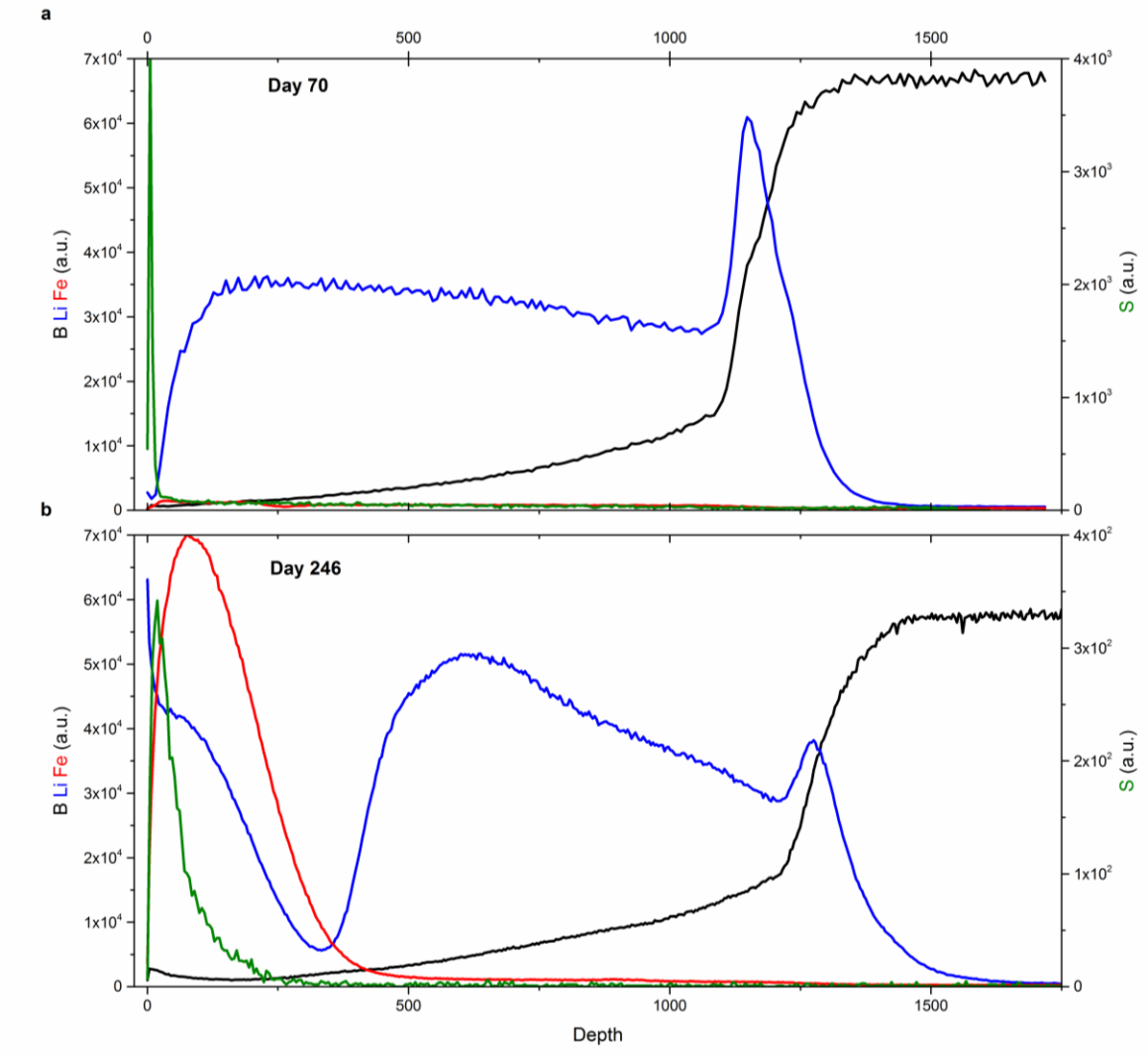


Figure 10: TOF-SIMS elemental profiles of polished surface of monoliths sampled at a) day 70 and b) day 246 after tracing experiment with LiCl (Li) and methylene blue (S). Significant changes are seen in the first 250 nm of the day 246 sample.

Discussion

Differences in alteration layer thicknesses

Analysis the alteration layers by multiple methods demonstrate the inconsistency between thicknesses derived from boron concentration in solution and those determined by analysis of the polished side by ToF-SIMS and TEM/SEM measurements. In the reference experiment, there was a slight increase in values determined by solution determination but values for all methods were within a 15% uncertainty. With the addition of magnetite a much larger discrepancy was seen between the methods as shown in Figure 11.

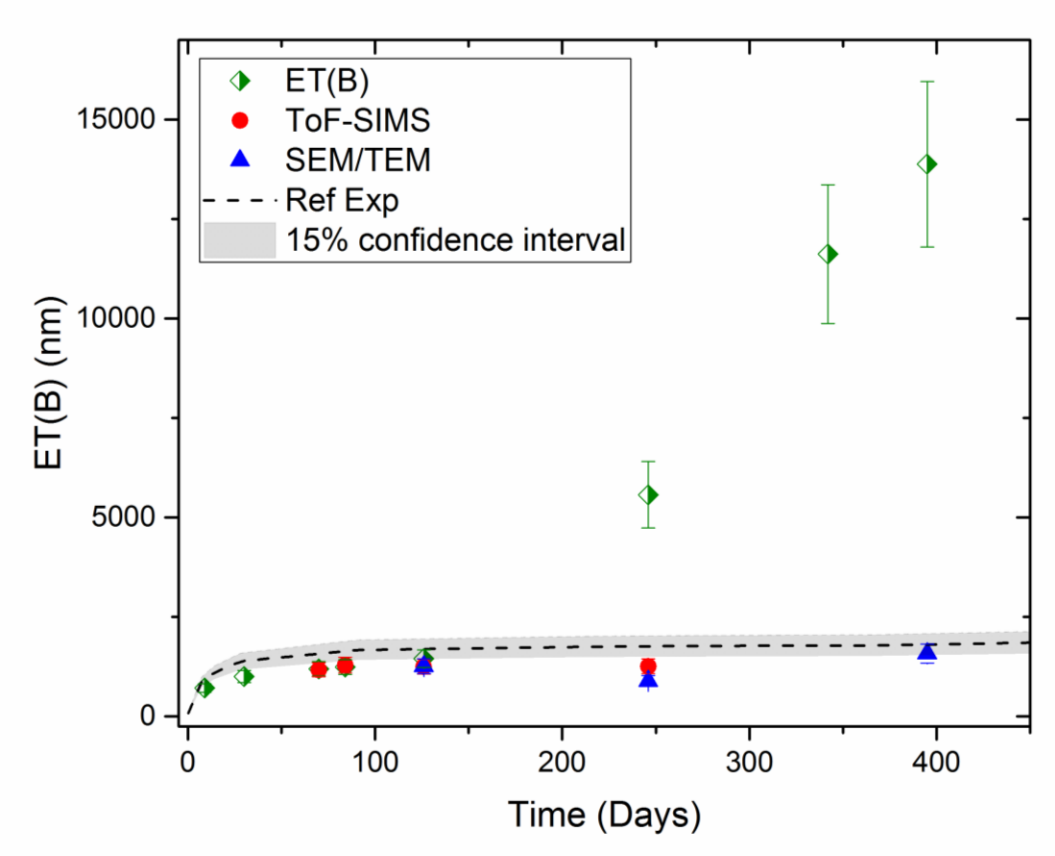


Figure 11: Comparison of alteration layer thickness measurements by technique. Agreement within all techniques is seen until after alteration resumed. Physical measurements of the polished side of the monolith remain in agreement with the reference

experiment. Changes determined by increased concentrations of boron in solution highlight the effect of the alteration at surface cracks on the non-polished sides. Dotted line represents the alteration layer thicknesses determined in the reference experiment along with a 15% confidence interval.

The three methods show agreement up until the rate resumption. Even after this time there is not a significant change in the alteration layer thickness of the polished side that was analyzed by ToF-SIMS and SEM/TEM; the alteration layer thicknesses remain within error of the reference experiment even after the resumption of alteration. In similar experiments [28,29] a correction factor was included to account for the different rate of alteration of the rough non polished surfaces. This experiment shows the exaggerated effects from these experiments that did not contain magnetite. It appears that the rough or as cut surfaces show preferential alteration over the polished side. These reference experiments showed that the non-polished surfaces contributed to a surface area 1.7x larger than that of just geometric considerations. This correction is applicable to the first regime in the absence of magnetite. But even factoring in this difference, it does not explain the factor 15 difference in the thicknesses (up to a factor 70 locally) obtained by solid and solution analysis. Moreover, a slight decrease of silicon concentration was seen between day 126 and day 246 but since the alteration layer should already be depleted in boron it does not explain this difference. It was found that the non-polished side had areas of large alteration that were centered on cracks in the surface that could begin to explain the discrepancies in thickness measurements.

Mechanisms of iron interaction

Many of the mechanisms detailed in Rebiscoul et al 2015 were seen in the work, although it is difficult to distinguish between Si sorption and SiO_2 precipitation by methods used in this experiment. It has to be assumed that both of these mechanisms (sorption and precipitation) were observed since the consumption of Si from solution was higher than can be

accounted for by sorption only. The sorption capacity for magnetite has been measured to be 19 ± 14 µmol of Si per gram of magnetite [47]. In this experiment this sorption capacity only allows for 7-80 ppm of Si (allowing for the large error within the measurement provided by Philippini et al) of the 120 ppm loss seen over the first two months after the addition of magnetite. Since the mechanisms of sorption and SiO_2 cannot be separated, it can be speculated that sorption takes place within the first day after magnetite was added to the system. Approximately 60 ppm of silica was lost from solution from day 70 to day 71 which falls within the range of 7 – 80 ppm that can be accounted for by the sorption capacity. Thus, both sorption and SiO_2 precipitation mechanisms that occur at the magnetite surface seem to predominate in the initial stages with the formation of secondary phases or a layer of iron at the glass surface seen only at the later time points in the experiment.

In an additional experiment, ISG grains of approximately 5 µm in diameter were altered in the same conditions as those tested here (pH 7, 90 ºC, solution at equilibrium with amorphous silica) until 100% of boron had been released (complete alteration of the glass grains). This left grains that can be thought of as pure alteration layer. The solubility of these altered grains were then measured, and after 100 days the system reached an equilibrium with a concentration of 43 ppm of Si at pH 7. It can be seen in our data that when the concentration of Si in this experiment reached levels below this threshold the alteration of the glass surface resumed. This is also evident from the isotopic concentrations of Si in solution. After this threshold value of Si was reached, the glass, containing primarily ^{28}Si, begins to alter to reestablish the equilibrium in solution; this can be seen with the increase of ^{28}Si over ^{29}Si at day 246.

Monitoring the diffusion of methylene blue and LiCl also gave insights into if the incorporation of exogenous elements such as iron changed the properties of the alteration layer. It is possible that the introduction of iron into the alteration layer could reduce the porosity of the

alteration layer and thus affect the ability of ions to diffuse. The GRAAL model predicts that the durability glass waste form is tied the thermodynamic stability the transport properties of the passivating layer [14]. While we know that iron is detrimental to the durability glass, a layer that would restrict iron diffusion would be considered protective over time. But as shown in figure 11, the iron rich layer did not limit the ability of small ions, Li in this case, to diffuse up and into the pristine glass layer. Thus under these conditions, iron only decreases the stability of the system without providing any protective effect.

Effects of surface cracks

As discussed above there is a large difference seen in the calculated alteration layer thickness by boron released and observed on the monolith. This was due to the propagation of alteration within the cracks on the rough surfaces, a phenomenon that was unexpected when this study was designed. While the alteration layer on the polished side remained the same thickness as seen in the experiment conducted by Gin et al 2015 of approximately 1 µm, the zones of alteration around the cracks extended up to 60 – 70 µm as shown in Figure 8. The effects of these cracks must carefully be considered since actual waste packages are expected to have many cracks due to cooling of the glass and any possible stress fractures from movement of the canister [48]. Though cracks within glass have been studied though not many studies have been directly related to nuclear glasses under repository conditions [48,49]. These cracks substantially increase the surface area of the glass block along with providing areas with unique chemical environments. The localized conditions within these cracks provide a preferential site for quick alteration.

Stress fractures on the rough surfaces of the monoliths were also seen in the reference experiment [28] yet alteration progressed quicker when in the presence of magnetite than seen previously. This could be due to the quick change in solution conditions when magnetite was added to the system. Within the first two months after the addition of magnetite the

concentration on silicon decreased from a steady state of about 140 ppm to around 20 ppm with a decrease in 60 ppm seen in the first day. This extreme change in solutions caused the resumption of alteration and it was the surface cracks that provided sites for this alteration to reestablish the equilibrium between solution and the glass matrix.

Several studies have shown that unique chemical environments exist within these cracks. [50,51] showed that there is an increase in diffusion constants of ions, specifically Na, within the cracks as compared to the bulk glass. The diffusion of these ions also creates a condensate region at the surface of the glass around the cracks. The pH in these regions increases compared to bulk solution which can lead to regions of increased silicate ion formation due to hydrolysis [52]. So it is not specific to glasses in contact with iron that these cracks form, but the iron can take advantage of these areas with unique chemistry as compared to the bulk which facilitates large regions of alteration that were not seen on the time scale of the reference experiment. Since the rate of propagation increases with the increase in crack length [53] the formation of these areas could be detrimental to the overall durability of the bulk glass.

Methods

Experimental Set-up

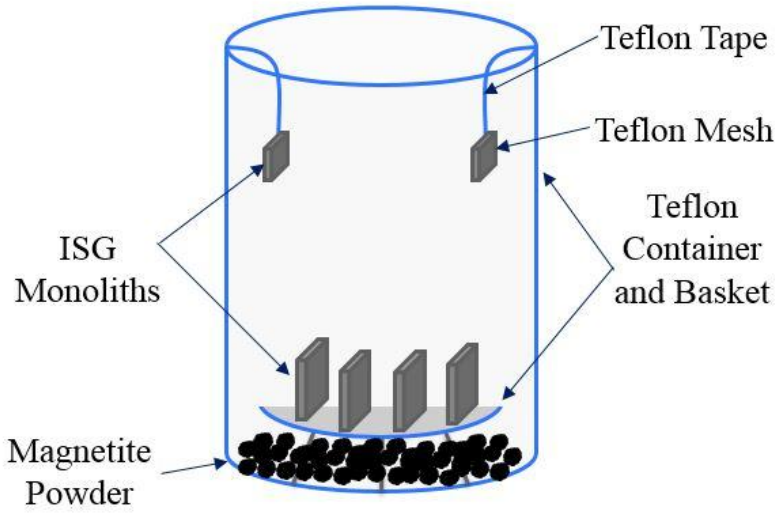
The ISG glass was prepared by MoSci Corporation (Rollo, MO, USA). The composition is given in Table 1.

International Simple Glass (ISG)

Oxide	Wt %
SiO_2	56.2
B_2O_3	17.3
Na_2O	12.2
Al_2O_3	6.1
CaO	5.0
ZrO_2	3.3

Table 2: Composition of JSG

The glass was initially melted into ingots using platinum-rhodium crucibles at 1300 °C for about 4 hours. The ingots were then annealed for 6 hours at 569 °C then cooled to room temperature at a rate of 50 °C per hour. From one ingot, 8 monoliths of 2.00 x 2.00 x 0.11 cm^3 and 8 monoliths of 0.50 x 0.50 x 0.11 cm^3 were obtained. One of the large faces of the monoliths were then polished to a mirror finish. The 8 large monoliths were put into a Teflon holder and placed in the bottom of a 250 mL Teflon vessel in a vertical orientation. The smaller monoliths were wrapped in Teflon mesh and hung into solution from the top of the vessel as shown in Figure 12.



407

408 *Figure 12: Schematic of experimental set - up. Magnetite powder was added into the vessel at day 70.*

409 The initial solution was saturated in amorphous $^{29}SiO_2$ (Eurisotop > 95% $^{29}SiO_2$) at $pH_{90°C}$
410 7. The isotopically tagged silica was melted with KOH (Suprapur) at 600°C and the resulting
411 soluble potassium silicate was then dissolved in 18 MΩ.cm H_2O to obtain a concentration of 141
412 ppm Si and 6900 ppm K. Due to a small initial concentration of additional cations (i.e. sodium
413 and calcium) an aliquot of the initial solution was characterized by Inductively Coupled Plasma
414 Optical Emission Spectroscopy (ICP-OES) for consideration of further calculations.

415 The resulting surface area was 76 cm^2 by geometric considerations. A previous study
416 has found that the resulting reactive surface area due to only one polished face of the monolith
417 is 1.7 x higher than the geometric surface area [29]; the resulting reactive SA was 129 cm^2. The
418 smaller monoliths contribute only a small fraction of the SA so these monoliths are used for
419 sampling throughout the experiment. The $pH_{90°C}$ of the solution was maintained at 7.0 ± 0.5 by
420 0.5 M KOH and 0.5 M HNO_3, and 90 °C, until around 6 months and was then let free to vary.

As the leaching solution was initially saturated with respect to amorphous silica, the glass was altered in a residual rate until day 70 at which time the system was perturbed. Approximately 9.3 g of magnetite (Sigma Aldrich 0.48 µm average particle size) was added.

Solution Analysis

The solution was sampled regularly throughout the experiment for cation concentrations analysis by ICP-OES and silicon isotope ratios by ICP-MS. All samples and standards were purified using BioRad AG50 X-12 (200-400 mesh) cation exchange resin before silicon isotope analysis, as described in detail by Georg et al [54]. Silicon isotope ratio measurements were performed on a Thermo Scientific Neptune Plus Multi-Collector Inductively Coupled Plasma Mass-Spectrometer (MC-ICPMS) at the Institut de Physique du Globe de Paris, France. All measurements were performed in static multicollection mode with Faraday cups attached to 10^{11} Ω amplifier resistors. The Faraday amplifier gains were calibrated daily before the analytical session, yielding long-term reproducibility better than 10 ppm. The instrument was operated at medium resolution to avoid polyatomic interferences (e.g. $^{14}N^{16}O$, $^{14}N_2$, $^{12}C^{16}O$) (Savage et al. 2013, Supplementary Material). The isotope beams of ^{28}Si, ^{29}Si and ^{30}Si were measured using L3, C and H3 cups, respectively. A tandem cyclone-Scott type spray chamber SIS (Stable Introduction System, Thermo Scientific) with a PFA micro-flow nebulizer (ESI, USA) was used as the introduction system.

Boron solution concentrations were obtained by ICP-OES and were used to calculate the normalized loss (NL), the equivalent thickness (*Eth*) and subsequent rates (*r*) along with the altered glass fraction (AGF). The calculation for normalized loss is shown in equation 4.

$$NL(B) = \frac{C_B \times V_{solution}}{\left((SA_{small} \times n_{small}) + (SA_{large} \times n_{large})\right) \times f_B} \qquad \text{Equation 4}$$

Where C_B is the concentration of boron in solution, V is the volume of solution, ρ is the density of glass which is 2.5 g.cm^{-3}, SA is the surface area of the glass, n is the number of monoliths

remaining, and f_B is the fraction of boron in the glass (0.0537). The surface area and volume values were changed throughout the experiment as monoliths were sampled and correcting for any evaporation in the system. The equivalent thickness calculation is shown in equation 5 which is the normalized loss divided by the density $\rho_{glass.}$

$$Eth(B) = \frac{NL(B)}{\rho_{glass}} \qquad \text{Equation 5}$$

The glass dissolution rate is then calculated as shown in equation 6. This is determined by using a three point linear regression.

$$r = \frac{d(Eth(B))}{dt} \qquad \text{Equation 6}$$

The altered glass fraction (AGF) is determined by equation 7.

$$AGF = \frac{C_B}{f_B \times (V_{glass} \times \rho_{glass})} \qquad \text{Equation 7}$$

Where C_B is the concentration of boron in solution in g, f_B is the fraction of boron in the glass (0.0537) and V_{glass} is the addition of volume from each glass monolith in cm^3.

The associated uncertainties for *NL* is 10%, *Eth* is 15%, while *r* is 30%.

The surface area is that the geometric surface area alone does not take into account the physical surface area of the monolith. A factor of 1.7x the geometric surface area is used to correct for surface roughness of the unpolished surfaces for the calculation of surface area of each monolith [29], as previously explained. Additionally, the propagation of cracks on the unpolished surfaces of the monolith provided additional water accessible areas that impact the overall alteration of the glass monolith. The phenomenon of alteration within these cracks will be discussed at greater depth within this paper.

462 Monoliths were sampled at multiple times throughout the experiment; day 70 (before
463 addition of magnetite, day 83 (approx. 2 weeks after addition), day 126 (approx. 2 months after
464 addition), day 246 (approx. 6 months after addition) and day 358 (approximately 9.5 months
465 after addition). These monoliths were cut into four pieces for different analyses.

466 The polished face of the first four monoliths were analyzed by TOF-SIMS (IONTOF TOF
467 5) to visualize elemental profiles within the alteration layer. Two sputtering beams were used
468 O_2^+ (50 x50 um^2 area) or Cs^+ (40 x 40 um^2 area). The Cs^+ beam was used to analyze the H, and
469 S ions while O_2^+ was used for all other ions. To minimize the matrix effects, all ions are
470 normalized to Zr as this element is immobile during alteration [55].

471 The day 246 monolith was also analyzed by TEM. A thin section was extracted from the
472 polished face of the sample and milled up to a thickness of ~100 nm. The sample was sputtered
473 with an Au/Pd mixture and coated with Pt for protection. Observations and analyses were
474 carried out with a Technai G2 (FEI) TEM microscope equipped with a LaB6 source operating at
475 200kV. A GATAN CCD camera, a BF-DF detector and an EDX detector EDAX Genesis were
476 used. The spatial resolution was 0.27 nm and the EDS spot size of 5 and 10 nm. For EDX
477 analysis, the sample was tilted of 20° to minimize the overlaying of different phases. The
478 counting time was 20 seconds to limit evaporation of mobile elements. SEM-EDS (JEOL JXA-
479 8500 F) was also used to observe the alteration layers and surface features of the day-126
480 (polished face) and the day-358 (as cut face) monoliths.

481 A post-experiment tracing was performed on the monoliths withdrawn at day 70, 83,126,
482 and 246. The monoliths were placed in a saturated amorphous $^{28}SiO_2$ at pH 7 at room
483 temperature for 100 hours. The solution also contained 4.4 x 10^{-4} $mol.L^{-1}$ methylene blue and
484 0.1 $mol.L^{-1}$ LiCl. TOF-SIMS was performed on the polished face of the samples to study the
485 diffusivity of these aqueous species into the developing alteration layers. This allowed for

comparison to the reference sample to further understand the influence of iron on the properties of the alteration layer.

Acknowledgements

This research was performed using funding received from the DOE Office of Nuclear Energy's Nuclear Energy University Program under Project 23-3361 in addition to funding provided by the CEA, Areva, and the Chateaubriand Fellowship from the Embassy of France in the U.S. Authors warmly thank Alkis Gourgiotis from IRSN, France for MC-ICP-MS analyses, Laurent Dupuy at Biophy Research, France for the TOF-SIMS analysis, Martiane Cabié at Aix-Marseille University,France for assistance with TEM, and CEA technical staffs for SEM analyses.

References

1. Donald, I. Waste Immobilization in Glass and Ceramic Based Hosts: Radioactive, Toxic and Hazardous Wastes. (Wiley, 2010).
2. ANDRA (Agence Nationale pour la gestion des Déchets RAdioactifs). Dossier 2005: Andra research of the geological disposal of high-level long-lived radioactive waste. Results and perspective. (2005).
3. Gin, S. et al. An international initiative on long-term behavior of high-level nuclear waste glass. Mater. Today **16,** 243–248 (2013).
4. Vienna, J. D., Ryan, J. V., Gin, S. & Inagaki, Y. Current Understanding and Remaining Challenges in Modeling Long-Term Degradation of Borosilicate Nuclear Waste Glasses. Int. J. Appl. Glass Sci. **4,** 283–294 (2013).
5. Andriambololona, Z., Godon, N. & Vernaz, E. R7T7 nuclear glass alteration in a saline medium: in situ experiments in the WIPP project. Appl. Geochem. **7,** 23–32 (1992).
6. Jollivet, P. et al. Effect of clayey groundwater on the dissolution rate of the simulated nuclear waste glass SON68. J. Nucl. Mater. **420,** 508–518 (2012).

7. Fleury, B. et al. Development of an Experimental Design to Investigate the Effects of R7T7 Glass Composition on the Residual Rate of Alteration. Procedia Mater. Sci. **7,** 193–201 (2014).
8. Frugier, P., Martin, C., Ribet, I., Advocat, T. & Gin, S. The effect of composition on the leaching of three nuclear waste glasses: R7T7, AVM and VRZ. J. Nucl. Mater. **346,** 194–207 (2005).
9. Gin, S., Beaudoux, X., Angéli, F., Jégou, C. & Godon, N. Effect of composition on the short-term and long-term dissolution rates of ten borosilicate glasses of increasing complexity from 3 to 30 oxides. J. Non-Cryst. Solids **358,** 2559–2570 (2012).
10. Jantzen, C. M., Brown, K. G. & Pickett, J. B. Durable Glass for Thousands of Years. Int. J. Appl. Glass Sci. **1,** 38–62 (2010).
11. Pierce, E. M. et al. Experimental determination of the effect of the ratio of B/Al on glass dissolution along the nepheline (NaAlSiO4)–malinkoite (NaBSiO4) join. Geochim. Cosmochim. Acta **74,** 2634–2654 (2010).
12. Pierce, E. M., Rodriguez, E. A., Calligan, L. J., Shaw, W. J. & Pete McGrail, B. An experimental study of the dissolution rates of simulated aluminoborosilicate waste glasses as a function of pH and temperature under dilute conditions. Appl. Geochem. **23,** 2559–2573 (2008).
13. Werme, L. O., Hench, L. L., Nogues, J.-L., Odelius, H. & Lodding, A. On the pH dependence of leaching of nuclear waste glasses. J. Nucl. Mater. **116,** 69–77 (1983).
14. Frugier, P. et al. SON68 nuclear glass dissolution kinetics: Current state of knowledge and basis of the new GRAAL model. J. Nucl. Mater. **380,** 8–21 (2008).
15. Grambow, B. & Muller, R. First-order dissolution rate law and the role of surface layers in glass performance assessment. J. Nucl. Mater. **298,** 112–124 (2001).
16. McGrail, B. P., Ebert, W. L., Bakel, A. J. & Peeler, D. K. Measurement of kinetic rate law parameters on a Na□Ca□Al borosilicate glass for low-activity waste. J. Nucl. Mater. **249,** 175–189 (1997).

17. Libourel, G. et al. The use of natural and archeological analogues for understanding the long-term behavior of nuclear glasses. Comptes Rendus Geosci. **343,** 237–245 (2011).
18. Parruzot, B., Jollivet, P., Rébiscoul, D. & Gin, S. Long-term alteration of basaltic glass: Mechanisms and rates. Geochim. Cosmochim. Acta **154,** 28–48 (2015).
19. Verney-Carron, A., Gin, S., Frugier, P. & Libourel, G. Long-term modeling of alteration-transport coupling: Application to a fractured Roman glass. Geochim. Cosmochim. Acta **74,** 2291–2315 (2010).
20. Doremus, R. H. Interdiffusion of hydrogen and alkali ions in a glass surface. J. Non-Cryst. Solids **19,** 137–144 (1975).
21. Doremus, R. H. Diffusion-controlled reaction of water with glass. J. Non-Cryst. Solids **55,** 143–147 (1983).
22. Boksay, Z., Bouquet, G. & Dobos, S. Diffusion Processes in Surface Layers of Glass. Phys. Chem. Glas. **8,** 140- (1967).
23. Ojovan, M. I., Pankov, A. & Lee, W. E. The ion exchange phase in corrosion of nuclear waste glasses. J. Nucl. Mater. **358,** 57–68 (2006).
24. Hench, L. Physical chemistry of glass surfaces. J. Non Cryst. Solids **25,** 343–369 (1977).
25. Techer, I., Advocat, T., Lancelot, J. & Liotard, J. M. Dissolution kinetics of basaltic glasses: control by solution chemistry and protective effect of the alteration film. Chem. Geol. **176,** 235–263 (2001).
26. Van Iseghem, P. et al. in Environmental Issues and Waste Management Technologies in the Materials and Nuclear Industries XII (eds. Cozzi, A. & Ohji, T.) 115–126 (John Wiley & Sons, Inc., 2009).
27. Geisler, T. et al. Aqueous corrosion of borosilicate glass under acidic conditions: A new corrosion mechanism. J. Non-Cryst. Solids **356,** 1458–1465 (2010).
28. Gin, S. et al. Origin and consequences of silicate glass passivation by surface layers. Nat. Commun. **6,** 6360 (2015).

29. Gin, S. et al. The fate of silicon during glass corrosion under alkaline conditions: A mechanistic and kinetic study with the International Simple Glass. Geochim. Cosmochim. Acta **151,** 68–85 (2015).
30. Valle, N. et al. Elemental and isotopic (Si-29 and O-18) tracing of glass alteration mechanisms. Geochim. Cosmochim. Acta **74,** 3412–3431 (2010).
31. Fournier, M., Gin, S. & Frugier, P. Resumption of nuclear glass alteration: State of the art. J. Nucl. Mater. **448,** 348–363 (2014).
32. Gin, S., Godon, N., Mestre, J. P., Vernaz, E. Y. & Beaufort, D. Experimental investigation of aqueous corrosion of R7T7 nuclear glass at 90°C in the presence of organic species. Appl. Geochem. **9,** 255–269 (1994).
33. Rebiscoul, D. et al. Reactive transport processes occurring during nuclear glass alteration in presence of magnetite. Appl. Geochem. **58,** 26–37 (2015).
34. Ribet, S. & Gin, S. Role of neoformed phases on the mechanisms controlling the resumption of SON68 glass alteration in alkaline media. J. Nucl. Mater. **324,** 152–164 (2004).
35. Reiser, J. et al. Glass Corrosion in the Presence of Iron-Bearing Materials and Potential Corrosion Suppressors. MRS Proc. **1744,** (2015).
36. Bildstein, O., Trotignon, L., Perronnet, M. & Jullien, M. Modelling iron–clay interactions in deep geological disposal conditions. Phys. Chem. Earth Parts ABC **31,** 618–625 (2006).
37. Burger, E. et al. Impact of iron on nuclear glass alteration in geological repository conditions: A multiscale approach. Appl. Geochem. **31,** 159–170 (2013).
38. Dillmann, P., Gin, S., Neff, D., Gentaz, L. & Rebiscoul, D. Effect of natural and synthetic iron corrosion products on silicate glass alteration processes. Geochim. Cosmochim. Acta **172,** 287–305 (2016).
39. Godon, N., Gin, S. & Frugier, P. SON68 Glass Alteration Enhanced by Magnetite. Procedia Earth Planet. Sci. **7,** 300–303 (2013).

40. McVAY, G. L. & Buckwalter, C. Q. Effect of Iron on Waste-Glass Leaching. J. Am. Ceram. Soc. **66,** 170–174 (1983).
41. Michelin, A. et al. Archeological slag from Glinet: An example of silicate glass altered in an anoxic iron-rich environment. Chem. Geol. **413,** 28–43 (2015).
42. Michelin, A. et al. Silicate Glass Alteration Enhanced by Iron: Origin and Long-Term Implications. Environ. Sci. Technol. **47,** 750–756 (2013).
43. Kittel, C. Introduction to Solid State Physics. (John Wiley & Sons, Inc., 2005).
44. Hed, P. & Edwards, D. Optical Glass Fabrication Technology. 2: Relationship Between Surface Roughness and Subsurface Damage. Appl. Opt. **26,** 4677–4680 (1987).
45. Preston, F. W. The Structure of Abraded Glass Surfaces. Trans. Opt. Soc. **23,** 141–164 (1922).
46. Griffith, A. A. The Phenomena of Rupture and Flow in Solids. Philos. Trans. R. Soc. Lond. Ser. Contain. Pap. Math. Phys. Character **221,** 163–198 (1921).
47. Philippini, V., Naveau, A., Catalette, H. & Leclercq, S. Sorption of silicon on magnetite and other corrosion products of iron. J. Nucl. Mater. **348,** 60–69 (2006).
48. Mallet, C., Fortin, J., Guéguen, Y. & Bouyer, F. Evolution of the crack network in glass samples submitted to brittle creep conditions. Int. J. Fract. **190,** 111–124 (2014).
49. Ougier-Simonin, A., Guéguen, Y., Fortin, J., Schubnel, A. & Bouyer, F. Permeability and elastic properties of cracked glass under pressure. J. Geophys. Res. Solid Earth **116,** B07203 (2011).
50. Celarie, F., Ciccotti, M. & Marlière, C. Stress-enhanced ion diffusion at the vicinity of a crack tip as evidenced by atomic force microscopy in silicate glasses. J. Non-Cryst. Solids **353,** 51–68 (2007).
51. Wiederhorn, S. M., Guin, J.-P. & Fett, T. The Use of Atomic Force Microscopy to Study Crack Tips in Glass. Metall. Mater. Trans. A **42,** 267–278 (2010).
52. Wiederhorn, S. M., Fett, T., Guin, J.-P. & Ciccotti, M. Griffith Cracks at the Nanoscale. Int. J. Appl. Glass Sci. **4,** 76–86 (2013).

53. Freiman, S. W., Wiederhorn, S. M. & Mecholsky, J., John J. Environmentally Enhanced Fracture of Glass: A Historical Perspective. J. Am. Ceram. Soc. **92,** 1371–1382 (2009).
54. Georg, R. B., Reynolds, B. C., Frank, M. & Halliday, A. N. New sample preparation techniques for the determination of Si isotopic compositions using MC-ICPMS. Chem. Geol. **235,** 95–104 (2006).
55. Cailleteau, C. et al. Insight into silicate-glass corrosion mechanisms. Nat. Mater. **7,** 978–983 (2008).